electronics

MDPI

Review

Recent Advances in Perfusion Assessment in Clinical Oncology Using Hyperspectral Imaging

Rok Hren [1,2,3,*], Tamás Dóczi [1], Erika Orszagh [1] and Dušan Babič [4]

[1] Syreon Research Institute, 1142 Budapest, Hungary
[2] Faculty of Mathematics and Physics, University of Ljubljana, 1000 Ljubljana, Slovenia
[3] Institute of Mathematics, Physics, and Mechanics, 1000 Ljubljana, Slovenia
[4] Aresis, d.o.o., 1000 Ljubljana, Slovenia
* Correspondence: rok.hren@fmf.uni-lj.si

Abstract

Perfusion assessment is critical in clinical oncology, particularly in tumor characterization, intraoperative decision making, and postoperative outcome predictions. Hyperspectral imaging (HSI) has emerged as a promising, non-contact, non-invasive, and contrast-free modality capable of capturing spatial and spectral information related to tissue oxygenation and hemoglobin distribution. This study provides an up-to-date review of recent advances in the use of HSI for perfusion monitoring in clinical oncological applications, with a special focus on its adoption in laparoscopic surgeries, brain tumor delineation, and head and neck cancer interventions. The integration of HSI into surgical workflows and its potential to reduce complications are discussed. Overall, while HSI is emerging as an appealing, real-time, quantitative perfusion imaging modality, a lack of standardized protocols and interpretation guidelines pose the most significant challenges. Addressing these gaps through multicenter clinical trials is essential for advancing the routine use of HSI in oncological surgery.

Keywords: hyperspectral imaging; oncology; clinical applications; literature review

Academic Editor: Krzysztof Wolk

Received: 30 July 2025
Revised: 25 August 2025
Accepted: 27 August 2025
Published: 28 August 2025

Citation: Hren, R.; Dóczi, T.; Orszagh, E.; Babič, D. Recent Advances in Perfusion Assessment in Clinical Oncology Using Hyperspectral Imaging. *Electronics* **2025**, *14*, 3439. https://doi.org/10.3390/electronics14173439

1. Introduction

Hyperspectral imaging (HSI) [1–5] combines imaging and spectroscopy to capture spatially resolved data across hundreds of contiguous spectral bands. Unlike conventional RGB or multispectral imaging, which measure only a few wavelengths, HSI provides a full spectrum at each pixel, enabling precise material identification through unique spectral "fingerprints" [6]. This powerful integration of spectral and spatial information has found applications in remote sensing, agriculture, environmental monitoring, food quality [1–5]; most recently, its uses have expanded into the biomedical sciences [7–27]. Its key advantages (non-contact, non-ionizing, and non-invasive acquisition that eliminates the need for contrast agents), along with its relatively low cost, straightforward hardware implementation, and ease of operation, make HSI particularly suitable for intraoperative surgical support, with the potential to enhance real-time clinical decision-making.

In oncology, HSI has demonstrated efficacy in detecting various types of carcinomas, particularly when combined with histopathological analysis [28–40]. The modality provides detailed information on physiological parameters such as tissue oxygenation, water content, and hemoglobin concentration [41], enabling the detection of clinically relevant changes including angiogenesis and hypermetabolism. With ongoing advancements in the

construction, calibration, and validation of HSI systems (e.g., [42,43]), the technique has emerged as a valuable tool for quantifying perfusion changes during clinical interventions in oncology.

In our previous reviews [44,45], we assessed early clinical studies that applied HSI to solid tumors across various anatomical sites, including the kidneys [46], eye [47], breasts [48,49], brain [50–53], and gastrointestinal tract [54–66]. Given the rapid evolution of clinical applications of HSI in oncology, an updated review is warranted. This article focuses, inter alia, on recent developments in laparoscopic HSI, brain tumor delineation, and head and neck cancer applications, all of which represent significant advances in the integration of HSI into oncological clinical practice. The review is written from a clinical perspective.

2. Materials and Methods

A comprehensive literature search was conducted on 9 June 2025 using PubMed and Scopus, without language restrictions, limited to studies published after 3 October 2022 (the cutoff of our prior review [44]). Studies were eligible if they applied HSI in a clinical oncological setting, meaning that animal, phantom, ex vivo, developmental, or purely methodological investigations were excluded, as well as reviews. Duplicate records were removed both within and across databases. When identical work was published first in conference proceedings and later in a peer-reviewed journal, the proceedings version was treated as a secondary report and discarded. Included studies were subsequently categorized according to the anatomical site of the tumor. Due to the heterogeneity of the studies, we adopted the format of a narrative review. A more detailed description of the methodology, including PICOS, search strings, and inclusion and exclusion criteria during title/abstract and full-text screening, is reported in Appendix A.

3. Results

A comprehensive literature review was conducted to find potentially relevant articles from MEDLINE/PubMed and Scopus databases (see Appendix A). A total of 1064 records were identified (PubMed: 186, Scopus: 878). After removing 192 duplicates, 872 records were screened by title and abstract. Of these, 808 were excluded as irrelevant, leaving 64 articles for full-text assessment, of which 29 met the inclusion criteria and were selected for data extraction. To ensure that no recently published or poorly indexed studies were missed, a brief, targeted supplementary search was performed after the primary PubMed and Scopus search: five additional records were retrieved. In total, 34 studies (29 from database searches and 5 from supplementary sources) [67–100] constitute the evidence base of the review. The process of study identification, screening, and inclusion is illustrated in the PRISMA flow chart (Figure 1). This diagram provides a step-by-step summary of the number of records retrieved, screened, excluded, and finally included in the evidence base.

As in our previous review, the selected studies were systematically organized according to tumor anatomical locations. Additionally, we briefly summarized in narrative format particularly relevant recent non-oncological, methodological or animal studies; however, these studies are not included in Table 1.

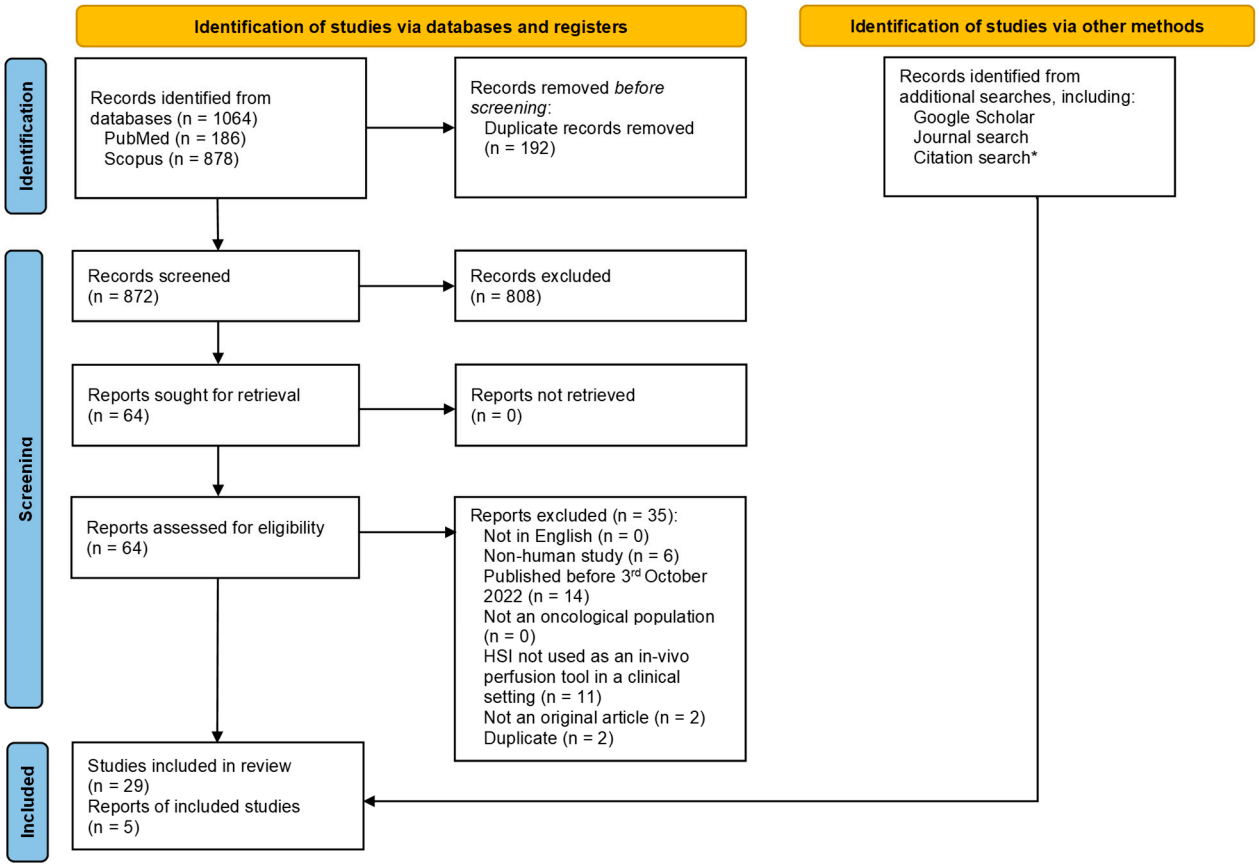

Figure 1. PRISMA flow chart of the rapid review.

3.1. Kidneys

Ayala et al. used HSI combined with deep learning for ischemia monitoring in laparoscopic surgery during partial nephrectomy [67]. Their system operated at video rate (25 Hz), leveraging a lightweight, compact HSI camera that integrated into existing surgical workflows. The authors addressed the high variability observed between patients by proposing a personalized deep-learning-based method, employing an ensemble of invertible neural networks (INNs) to detect ischemia as an out-of-distribution problem. A clinical study involving 10 patients demonstrated that their approach differentiated between perfused and ischemic kidney tissue with high accuracy, achieving a median/mean area under the receiver operating curve (AU-ROC) of 1.0/0.9. Future research should include explorations of infrared imaging to enhance tissue penetration and further refining the clinical integration of HSI technology into surgical workflow.

An important methodological study was published by Studier-Fischer et al. [101], who also used HSI combined with artificial intelligence to assess intraoperative renal perfusion, a critical factor for preserving organ function during kidney surgeries such as partial nephrectomy or transplantation. Employing a controlled porcine model, the authors evaluated HSI under the conditions of complete, gradual, and partial kidney malperfusion, distinguishing various perfusion states such as physiological, avascular, arterial ischemia, and venous congestion. Notable differences were observed in spectral reflectance and oxygen saturation (StO_2) [41] among these states. Machine learning algorithms demonstrated high accuracy (97.8%) in differentiating perfusion conditions. The animal data showed potential clinical transferability when compared to human kidney transplantation data.

Table 1. Articles included in the review that reported the use of hyperspectral imaging (HSI) to quantify perfusion changes in clinical oncology applications since 3 October 2022 [67–100]. DIEP—deep inferior epigastric perforator; CIN—cervical intraepithelial neoplasia; IDH—isocitrate dehydrogenase; SCC—squamous cell carcinoma; SMF—submucous fibrosis; BCC—basal cell carcinoma; AK—actinic keratosis; SK—seborrheic keratosis; NSCLC—non-small-cell lung cancer; SCLC—small-cell lung cancer. In terms of methodology, several studies employed HSI combined with machine learning and deep learning approaches to improve tissue differentiation and perfusion assessment, such as Ayala et al. using invertible neural networks (INNs) for ischemia detection in nephrectomy [67], Leon et al. applying multiple classifiers for intraoperative brain tumor detection [74], and Bali et al. integrating endoscopic HSI with CNN-based analysis for head and neck cancers [81]. Others focused on comparative imaging modalities, such as Kleiss et al. combining HSI with ICG-fluorescence angiography and thermal imaging for flap perfusion [68], or Zimmermann et al. evaluating HSI for colon interposition after esophagectomy [95]. A subset of studies explored hardware innovations such as snapshot HSI integrated into surgical microscopes (Giannantonio et al. [75]; Puustinen et al. [76]) or augmented reality systems for real-time intraoperative guidance (Sancho et al. [73]). Collectively, these methodological advances illustrate the trend toward multimodal imaging, integration into surgical workflows, and the increasing role of neural networks for spectral–spatial interpretation. In terms of outcomes, the evidence demonstrates that HSI consistently provided quantitative perfusion metrics (StO_2, THI, TWI, NIR-PI) that correlated with clinical endpoints, including flap viability [82,83], anastomotic integrity [96–98], and postoperative complications [87]. In oncological resections, HSI supported more accurate tumor delineation, particularly in neurosurgery (Marois et al. [72]; Martín-Pérez et al. [79]) and head and neck surgery (Pertzborn et al. [80]; Chand et al. [84]), while, in dermatology, it enabled discrimination between benign and malignant lesions (Calin et al. [89]; Courtenay et al. [93,94]; Huang et al. [92]). Importantly, studies such as Bannone et al. [88] demonstrated the feasibility of real-time, automatic tissue recognition in large patient cohorts, suggesting future scalability. Across these outcomes, HSI showed potential to improve intraoperative decision-making, reduce complications, and serve as a non-invasive, label-free alternative to established imaging modalities.

Reference	Year of Publication	Number of Patients	Oncologic Intervention
Kidneys			
Ayala et al. [67]	2023	10	Partial nephrectomy
Eye			
No new studies in the clinical oncological setting (since 3 October 2022)			
Breasts			
Kleiss et al. [68]	2024	15	DIEP flap breast reconstruction surgery
Kondziołka et al. [69]	2024	26	Skin response to radiation
Female reproductive system			
Schimunek et al. [70]	2023	41	CIN
Vega et al. [71]	2025	62	CIN and cervical cancer
Brain			
Marois et al. [72]	2023	1	Glioma resection
Sancho et al. [73]	2023	5	Brain tumor resection
Leon et al. [74]	2023	34	Brain tumor resection
Giannantonio et al. [75]	2023	5	Low-grade glioma resection
Puustinen et al. [76]	2023	1	High-grade glioma resection
MacCormac et al. [77]	2023	1	Posterior fossa meningioma
Kifle et al. [78]	2023	4	Epilepsy or malignant neoplasm (pediatric)
Martín-Pérez et al. [79]	2024	10	IDH-mutated tumors and other carcinoma
Head and neck			
Pertzborn et al. [80]	2022	7	Oral SCC
Bali et al. [81]	2024	12	Oral SCC
Felicio-Briegel et al. [82]	2024	14	Radial forearm free flap reconstructive surgery
Thoenissen et al. [83]	2023	13	Tumor resection in head and neck surgery
Chand et al. [84]	2024	91	Oral SMF, leukoplakia, and oral SCC
Xoxha et al. [85]	2025	16	SCC and BCC
Lungs			
Ellebrecht and Kugler [86]	2023	19	Adenocarcinoma NSCLC, squamous NSCLC, SCLC

Table 1. *Cont.*

Reference	Year of Publication	Number of Patients	Oncologic Intervention
Liver/abdominal organs			
Felli et al. [87]	2022	15	Hepatectomy
Bannone et al. [88]	2024	169	Elective abdominal surgery (pancreatoduodenectomy, total pancreatectomy, distal pancreatectomy, colectomy, splenectomy, sarcoma resection, major liver resection, minor liver resection, explorative laparotomy)
Skin			
Calin et al. [89]	2023	36	SCC, BCC, AK, and SK
Stridh et al. [90]	2024	1	Cutaneous angio-sarcoma
Parasca et al. [91]	2024	11	SCC and BCC
Huang et al. [92]	2024	34	Mycosis fungoides, psoriasis and atopic dermatitis
Courtenay et al. [93]	2024	125	SCC, BCC, and AK
Courtenay et al. [94]	2024	125	SCC, BCC, and AK
Gastrointestinal tract			
Zimmermann et al. [95]	2023	8	Esophagectomy—open surgery
Thomaßen et al. [96]	2023	19	Gastrointestinal resection—laparoscopic surgery
Ilgen et al. [97]	2024	22	Esophagectomy—laparoscopic surgery
De Winne et al. [98]	2025	2	Esophagectomy—laparoscopic surgery
Cardiovascular system			
Perkov et al. [99]	2024	6	Infantile hemangioma
Endocrine glands			
Waterhouse et al. [100]	2025	12	Transsphenoidal surgery of pituitary adenomas

3.2. Eye

No new clinical studies in the oncological setting were reported since our previous review. In the study of Merdasa et al. [102] oncological patients were excluded, while HSI combined with spectral unmixing was conducted for the real-time monitoring of StO_2 during reconstructive surgery using forehead skin flaps for brow ptosis, which may also arise due to, e.g., basal cell carcinoma (BCC), melanoma, actinic keratosis (AK), and squamous cell carcinoma (SCC). Spectral unmixing across a broad spectral range, accounting for the absorptive contributions of melanin, fat, collagen, and water, produced a more clinically accurate estimation of StO_2 than traditional methods, which typically consider only the spectral features of oxygenated (HbO_2) and deoxygenated (HbH) hemoglobin [41]. The results demonstrated a clear gradient in StO_2 maps of partially excised forehead flaps along the length of the flap, from approximately 95% at the base to around 85% at the tip, with StO_2 across the entire flap dropping rapidly (within minutes) to about 50% following flap excision.

3.3. Breasts

Kleiss et al. [68] assessed the perfusion of deep inferior epigastric perforator (DIEP) flaps in 15 patients using indocyanine green fluorescence angiography (ICG-FA), HSI, and thermal imaging (TI) following a standardized imaging protocol: perfusion curves and parameters were derived from ICG-FA, HbO_2 and HbH values from HSI, and flap temperatures from TI. Post hoc quantitative analysis of intraoperative ICG-FA data distinguished between adequately and insufficiently perfused DIEP flaps, identifying arterial inflow absence in two patients and venous outflow occlusion in one patient. Partial flap epidermolysis, detected postoperatively, could have been predicted intraoperatively via ICG-FA metrics. Postoperative HSI revealed impaired perfusion based on elevated HBH levels, while TI showed limited utility.

Kondziołka et al. [69] followed the study of Chin et al. [48] and evaluated the use of HSI for assessing acute radiation dermatitis (ARD) in 26 patients during breast radiation therapy. The main goal was to objectively quantify skin reactions by analyzing hemoglobin and melanin concentrations in irradiated skin areas. Using HSI within a 400–1000 nm spectral range, the researchers found a strong correlation between hemoglobin concentration and the severity of ARD as rated using the standard Common Terminology Criteria for Adverse Events (CTCAE) scale. The findings indicate that HSI can effectively quantify changes in skin composition due to radiation exposure, suggesting that hemoglobin could serve as a reliable biomarker for radiation-induced skin damage. No correlation was identified between chromophore distribution and CTCAE grading, possibly due to uniform irradiation.

3.4. Female Reproductive System

In the prospective study [70], the feasibility of a commercially available, medically approved HSI system was assessed to differentiate for cervical intraepithelial neoplasia (CIN) lesions from healthy cervical tissue in 41 patients with histologically confirmed CIN (grades 1–3). Significant spectral differences between CIN lesions and normal cervical tissue were demonstrated, especially within the wavelength range of 555–585 nm, with the most marked difference observed at 575 nm. These results suggest that HSI can reliably distinguish dysplastic from healthy tissue in a contact-free, marker-independent manner. Several limitations were noted and, for the methodology to be suitable for a clinical setup, advanced imaging solutions such as endoscopic adaptations and automated analytical methods incorporating machine learning would be needed.

Vega et al. [71] addressed some of those concerns in a feasibility study on using HSI as a colposcopic method for detecting precancerous cervical lesions. They employed a custom-built hyperspectral colposcope on 62 patients to distinguish between normal cervical tissue, various grades of CIN, and cervical cancer. The system showed high spatial and spectral accuracy and was integrated into routine clinical examinations, demonstrating potential to overcome current colposcopy limitations related to subjectivity and low diagnostic accuracy.

3.5. Brain

Marois et al. [72] introduced an HSI system using a birefringent spectral demultiplexer, specifically designed for the rapid intraoperative imaging of protoporphyrin IX (PpIX) during neurosurgery. This system simultaneously acquired 64 spectral channels, accelerating data acquisition compared to traditional liquid crystal tunable filter-based devices. Phantom experiments confirmed superior linearity and sensitivity at low fluorophore concentrations, with frame rates over 70-fold faster. Clinical application in a single patient during glioma resection demonstrated that the device produced accurate, real-time quantitative maps of PpIX concentration.

The study of Sancho et al. [73] presented an augmented reality (AR) system designed for real-time acquisition, processing, and visualization of HSI data during neurosurgical procedures, particularly brain tumor resections. It utilized an HSI snapshot camera combined with LiDAR technology, enabling neurosurgeons to differentiate tumor tissue from healthy areas with high spatial accuracy. The system processed data at approximately 14 frames per second, providing an immersive 3D AR visualization by overlaying hyperspectral classification maps onto RGB point clouds captured through LiDAR, enhancing surgical precision and decision-making. The approach leveraged GPU acceleration to maintain real-time performance and has been validated during actual surgical operations in five patients.

Leon et al. [74] investigated HSI combined with machine learning techniques as a tool for intraoperative brain tumor detection. Using 61 hyperspectral images from 34 patients, the authors applied multiple classification algorithms to distinguish between tumor tissue, normal tissue, and blood vessels. The approach achieved promising results, particularly when integrating both spatial and spectral information, reaching a macro F1-Score of approximately 70.2%, which points to the capability of HSI in accurately delineating tumor margins.

In a pilot study including fivev patients undergoing low-grade glioma resection, Giannantonio et al. [75] integrated an HSI with a snapscan camera (468–787 nm range) into a surgical microscope and combined it with a deep-learning-based method to assist surgeons intraoperatively [103]. Furthermore, they identified dominant spectral channels through neural networks to balance precision and speed, enabling real-time clinical application. Similarly, the feasibility study conducted by Puustinen et al. [76] addressed the integration of HSI systems into surgical microscopes during high-grade (grade 3) glioma resection in a single patient to provide the effective classification of brain tissues.

MacCormac et al. [77] developed a handheld intraoperative HSI system [104], which was tested in preclinical and clinical settings to evaluate its feasibility, safety, and effectiveness in a single patient presenting with posterior fossa meningioma. The device allowed for real-time, wide-field, label-free intraoperative tissue differentiation (meningioma, cerebellum, and surgical patty) by capturing spectral data across numerous wavelength bands (350–1000 nm). However, some technical limitations, such as image blur from handheld use and chromatic artifacts, were identified.

Kifle et al. [78] integrated a snapshot HSI camera into a surgical microscope and combined it with machine learning to differentiate between healthy brain tissue and lesions during pediatric brain tumor resections in four patients. They collected images using an RGB camera and two types of hyperspectral cameras: one in the visible spectrum and the other in the infrared spectrum. A random forest classifier successfully segmented the tissues, and, contrary to expectations, RGB imaging demonstrated the highest segmentation accuracy with an average intersection of union (IoU) of 0.76.

The study by Martín-Pérez et al. [79] evaluated and compared the performance of two HSI camera types—pushbroom (linescan) and snapshot—for identifying brain tissue and chromophores in vivo. Ten patients with isocitrate dehydrogenase (IDH)-mutated tumors and other brain pathologies were imaged, and spectral data from healthy and pathological tissues were analyzed. The researchers found that both cameras showed comparable spectral behaviors, although the pushbroom camera had higher spectral and spatial resolution but required a significantly longer acquisition time (~1 min 40 s) compared to the snapshot camera (100 ms). Despite the presence of more noise in snapshot camera data, particularly after normalization, its real-time imaging capability makes it suitable for surgical applications. Additionally, certain chromophore absorption peaks (oxidized cytochrome b, HbO_2, and water) could be identified with the linescan camera, supporting its utility for detailed spectral analysis during brain surgery.

A very recent methodological study by Roddan et al. [105] presented a multimodal imaging platform combining HSI and probe-based confocal laser endomicroscopy (pCLE) to enhance tumor identification during neurosurgery. This integrated approach addressed the individual limitations of each modality, providing real-time macroscopic tissue analysis (HSI) and cellular-level imaging (pCLE). The developed system demonstrated high spatial accuracy with minimal reprojection errors, and the combined use of HSI and pCLE improved tumor segmentation performance, particularly in terms of the Dice score and recall, compared to either modality alone.

3.6. Head and Neck

Pertzborn et al. [80] evaluated the potential of HSI when combined with machine learning for intraoperative tumor margin assessments in oral SCC. Using unstained tissue sections from seven patients, hyperspectral data were collected, processed, and analyzed through advanced machine learning models, including a 3D convolutional neural network (CNN). The approach demonstrated good accuracy (76%) and high specificity (89%) in differentiating tumor from healthy tissue, although sensitivity was relatively moderate (48%).

Their work was advanced in the study of Bali et al. [81], who evaluated the feasibility of using endoscopic HSI for the real-time visualization of tumor margins during head and neck cancer surgeries in 12 patients. Employing a medically approved CE-certified HSI camera, researchers optimized an intraoperative workflow to ensure quick and practical use during surgery. This approach enabled surgeons to visualize tumor boundaries in under 10 s per measurement, significantly enhancing accuracy (79%), sensitivity (72%), and specificity (84%) in differentiating tumor tissue from healthy tissue. The medical team became proficient with the system after only two surgeries, indicating the potential of HSI to be integrated into routine surgical procedures and reduce incomplete tumor resections.

Their methodology was recently expanded [106] via the ex vivo examination of an approach combining HSI and deep learning for intraoperative tumor margin assessment in six patients with head and neck SCC. The method involved capturing hyperspectral images of freshly resected tumor samples from multiple angles, constructing a three-dimensional model, and correlating these data with high-resolution 3D histological reconstructions. The integrated deep learning models (U-Net, UwU-Net, U-Net Transformer) demonstrated high accuracy (up to 98%) and sensitivity (93%) in distinguishing tumor from healthy tissue. This platform still requires clinical integration and validation.

Felicio-Briegel et al. [82] applied HSI to the postoperative monitoring of intraoral free flaps used in head and neck reconstruction. Perfusion indices included the Tissue Hemoglobin Index (THI), StO_2, Near-Infrared Perfusion Index (NIR-PI), and Tissue Water Index (TWI) [41]. Fourteen patients who underwent reconstructive surgery with radial forearm free flaps were monitored intraoperatively and postoperatively at defined intervals. The study found that StO_2 remained above critical thresholds intraoperatively (>50) and immediately postoperatively (>40) while significant differences were observed only in TWI between intraoperative and postoperative days 2 and 7–9. No flap loss occurred. Researchers did find some challenges related to imaging the oral cavity and proposed the use of an endoscopic version of HSI.

Thoenissen et al. [83] used HSI in their retrospective clinical study to evaluate the postoperative survival of free microvascular flaps following tumor resection in oral, maxillofacial, and facial (craniomaxillofacial) surgery. Thirteen patients with flap reconstructions were monitored using an HSI camera, assessing parameters StO_2, THI, TWI, and NIR-PI at standardized intervals from 3 to 100 h postoperatively; an additional 10 patients served as controls. HSI results varied between patients without significant intra-individual differences. After 24 h, mean decreases in StO_2 (16.77%), THI (9.16%), and TWI (8.46%) were observed, correlating well with clinical stability and no flap losses during the observation period.

Chand et al. [84] introduced a publicly available in vivo HSI dataset aimed at diagnosing various oral diseases: specifically, oral submucous fibrosis (SMF), leukoplakia, and oral SCC. Recognizing the limitations of ex-vivo imaging, such as tissue changes due to preservation, the authors employed a compact, state-of-the-art HSI snapshot camera capturing images in 16 spectral bands ranging from 460 to 600 nm. The dataset included 243 spectral images from 91 patients, carefully classified into different oral health conditions and accompanied by patient histories and annotations. Detailed image acquisition

and preprocessing methods were outlined, emphasizing the importance of accurate calibration, noise reduction, and labeling. The researchers validated image quality through spatial resolution and signal-to-noise ratio analyses, confirming high overall image quality suitable for clinical diagnostics.

Hoxha et al. [85] combined HSI with machine learning techniques for the non-invasive classification of skin lesions associated with SCC and BCC. Using various tissue indices derived from HSI, their objective was to differentiate between tumor, peritumoral, and healthy skin areas. The approach was tested on a dataset of 24 lesions from 16 patients. Results showed that tissue index images substantially improved classification accuracy (91.75%) compared to traditional RGB imaging (87.73%). The area under the curve (AUC) for distinguishing tumors from other regions increased significantly when using tissue indices (up to 0.96), indicating that HSI-derived parameters could provide biomarkers for tissue characterization and lesion classification.

The methodological study by Mostafa et al. [107] introduced tumor segmentation in head and neck cancer surgery using HSI combined with Graph Neural Networks (GNNs). Traditional machine learning methods primarily classify individual HSI pixels or tiles without spatial context, which may limit segmentation accuracy. This research addressed the challenge by employing GNNs to utilize spatial context across neighboring regions, enhanced by features extracted through CNNs. Furthermore, the authors developed a specialized quality-aware loss function that weights tiles based on local image quality metrics to mitigate the impact of low-quality data. Validation on an ex vivo dataset comprising 51 hyperspectral images from 30 patients demonstrated that the proposed CNN + GNN model outperforms conventional context-agnostic CNN methods.

3.7. Lungs

The prospective Stage 2a study (Clinicaltrials.gov: NCT04784884) by Ellebrecht and Kugler [86] evaluated the intraoperative use of HSI for assessing bronchus perfusion during pulmonary resections [108], specifically focusing on bronchus stump and anastomosis. Using tissue indices, researchers found that bronchus stumps exhibited reduced deeper tissue perfusion (NIR-PI) and hemoglobin levels (in terms of organ hemoglobin index OHI defined as THI/2 [109]), while upper tissue layer perfusion (StO_2) remained unchanged post-resection. Sleeve resection showed decreased perfusion both superficially (StO_2) and deeply (NIR-PI) in anastomosis regions compared to central bronchus areas. These outcomes show the potential of HSI as a real-time, non-invasive tool for assessing bronchus perfusion intraoperatively, potentially aiding in predicting and reducing complications such as bronchopleural fistulas.

3.8. Liver/Abdominal Organs

In the clinical trial (Clinicaltrials.gov: NCT04589884), Felli et al. [87] used HSI as an intraoperative tool for assessing liver perfusion and predicting post-operative complications following major hepatectomy. Conducted with 15 patients undergoing liver resections for malignant lesions, HSI measurements, including StO_2, TWI, NIR-PI, and OHI, were collected intraoperatively and analyzed in relation to short-term clinical outcomes and serum biomarkers. The results showed significant correlations: lower TWI was linked with post-operative reinterventions, lower OHI was linked with sepsis and liver failure, and StO_2 was negatively correlated with liver damage biomarkers (alanine transaminase—ALT). The findings suggest that HSI could provide real-time intraoperative guidance, potentially improving outcomes after major hepatic surgery.

Within the same clinical trial (ClinicalTrial.gov: NCT04589884) [88], HSI was combined with deep learning for automatic, real-time tissue recognition during abdominal

surgery, based on data from 169 patients across two centers. CNNs were trained to classify tissues into 13 categories. The results showed excellent accuracy for certain tissues such as skin (100%) and liver (97%), although some tissues with similar embryological origins or overlapping boundaries presented more challenges. Within-center validation achieved significantly better performance than cross-center validation, emphasizing the need for high-quality, multicentric datasets to ensure robust generalization and clinical translation. The authors suggest the integration of HSI into surgical workflows under the new framework named "surgical optomics", aiming at enhanced surgical precision through automatic tissue recognition.

3.9. Skin

Calin et al. [89] analyzed hyperspectral images from 36 patients with benign (seborrheic keratosis and AK) and malignant tumors (BCC and SCC). They defined a novel index called the hyperspectral-imaging-based skin cancer index (HSI-SCI), based on differences in the slopes of spectral reflectance curves between tumor and normal skin within a specific spectral range (580–600 nm). The HSI-SCI index successfully differentiated between benign and malignant tumors and even allowed for precise distinction between tumor subtypes without overlapping, correlating strongly with histopathological diagnosis.

Stridh et al. [90] combined non-invasive imaging modalities, laser speckle contrast imaging (LSCI), HSI, and photoacoustic imaging (PAI), to map the functional and molecular characteristics of an angiosarcoma in the periocular area. LSCI demonstrated increased perfusion in the tumor, indicative of its high vascularity, HSI revealed significantly higher total hemoglobin and reduced oxygen saturation within the tumor, suggesting the pooling of deoxygenated blood, and PAI, applied ex vivo, provided three-dimensional molecular composition maps, confirming findings from HSI and additionally demonstrating differences in collagen content. The integration of these methods was shown to offer detailed, complementary information that is potentially beneficial for preoperative tumor assessment.

Parasca et al. [91] explored HSI in the precise preoperative assessment of tumor margins in 11 histologically confirmed cases (6 BCCs, 5 SCCs). Hyperspectral data were segmented based on spectral and spatial features and classified using a Spectral Angle Mapper classifier. The method demonstrated high performance, achieving median AUC values of 0.8014 for SCCs, 0.8924 for BCCs, and 0.8930 for normal skin.

Huang et al. [92] combined snapshot HSI and artificial intelligence to accurately identify skin lesions, particularly mycosis fungoides (MF), a form of skin cancer, from psoriasis and atopic dermatitis. The research used a dataset comprising 1659 images of skin lesions from 34 patients to train a multi-stage diagnostic model, incorporating U-Net Attention for lesion segmentation, a hyperspectral model for feature extraction, and XGBoost for classification. The system effectively isolated and classified skin lesions, achieving high accuracy, with sensitivity of 90.72%, specificity of 96.76%, and an AU-ROC of 0.9351, thus demonstrating significant potential for the early-stage detection of MF and differentiation from benign inflammatory skin conditions.

In two studies, Courtenay et al. [93,94] evaluated near-infrared (NIR) HSI (900.6–1454.8 nm) combined with CNNs and support vector machines (SVMs) to classify non-melanoma skin cancer, including BCC, SCC, and AK. The methodology achieved overall accuracies above 80%, with specific tasks exceeding 90%. The best discrimination was observed between AK and other lesion types, while distinguishing between BCC and SCC was more challenging. Transfer learning from shorter wavelengths did not improve the results. Despite promising findings, the authors pointed out that further refinement of algorithms is required to reduce data noise before broader clinical application is feasible.

The methodological studies of Lin et al. [110,111] are worth mentioning. They evaluated the efficacy of a novel imaging algorithm, the Spectrum-Aided Vision Enhancer (SAVE), in detecting various types of melanoma, including acral lentiginous melanoma, melanoma in situ, nodular melanoma, and superficial spreading melanoma. The SAVE system converts RGB images into hyperspectral images. The researchers utilized different YOLO machine learning models (YOLO v5, YOLO v8, YOLO v9) and compared their performance between SAVE-generated and traditional RGB images. SAVE demonstrated superior performance across multiple metrics, including precision, recall, F1 score, and mean average precision. These findings indicate the clinical potential of SAVE in early melanoma detection.

3.10. Gastrointestinal Tract

A persistent limitation in gastrointestinal oncology has been the size of HSI cameras, which has largely confined their use to open surgery [54–66], most recently by Zimmermann et al. [95]. This barrier was addressed in the ex vivo evaluation of a laparoscopic HSI system [112], followed by two clinical feasibility studies that brought HSI into minimally invasive surgery.

In the first pilot study, Thomaßen et al. [96] compared a laparoscopic HSI system for minimally invasive surgery (HSI-MIS) with a well-established open-surgery platform (HSI-Open). Nineteen patients undergoing gastrointestinal resections were imaged intraoperatively, and perfusion parameters (StO_2, OHI, NIR-PI, and TWI) were analyzed. The mean absolute error between the two systems, after optimization with partial least-squares regression, ranged from $10.3 \pm 6.0\%$ to $12.6 \pm 5.2\%$, while the average root-mean-square error was 0.14 ± 0.06, indicating good agreement.

A subsequent pilot trial by Ilgen et al. [97] enrolled 21 patients undergoing robotic, total minimally invasive, or hybrid Ivor Lewis oesophagectomy and compared HSI-MIS results with those from 30 patients imaged using HSI-Open. Surgeons confirmed the feasibility of thoracoscopic and robotic acquisition but noted new challenges, including motion artefacts and the need to maintain a consistent 5–7 cm working distance. Perfusion metrics (StO_2, TWI, OHI) did not differ significantly between systems, although HSI-MIS tended to overestimate NIR-PI values.

Taken together, these pilot studies showed favorable concordance between laparoscopic and open HSI platforms, supporting the reliability of HSI-MIS for future clinical trials in minimally invasive gastrointestinal oncology.

De Winne et al. [98] built upon these findings as they integrated a snapshot HSI camera into a standard laparoscopic workflow to evaluate oxygenation at the gastric graft anastomotic site. In this proof-of-concept study involving two patients, they compared HSI-derived oxygenation values with traditional ICG-FA and capillary lactate measurements. HSI successfully identified regions of low oxygenation at the anastomosis, correlating with high lactate levels and the presence of anastomotic leakage (AL). Spectral differences in the 460–500 nm range enabled distinction between ischemic, perfused, and anastomotic tissue, with HSI showing greater spatial precision than ICG-FA. The study concluded that HSI could serve as a real-time, label-free, and more detailed alternative for assessing tissue perfusion and hypoxia, potentially reducing AL rates and enhancing surgical outcomes.

Another research group [113] is currently developing a prototype laparoscopic hyperspectral surgical system designed to provide real-time, quantitative StO_2 maps during gastrointestinal surgery; the research team has already validated the system in a live porcine model by correlating StO_2 values with those from a standard tissue oximetry probe and comparing oxygenation maps to ICG-FA during a simulated colorectal anastomosis.

An interesting clinical study [114], although not one focusing on perfusion assessment, explored the use of HSI as a method for detecting high levels of fecal occult blood directly on the stool surface, aiming to improve colorectal cancer screening. In a study of 100 patients undergoing colonoscopy, researchers developed a discriminant algorithm based on HSI and machine learning techniques, identifying blood levels exceeding a cutoff of 400 ng/mL. The algorithm demonstrated high sensitivity (83.3%), specificity (92.9%), and overall accuracy (90.8%), significantly outperforming conventional fecal occult blood tests by enabling the entire stool surface to be evaluated instantly and non-invasively. Verification tests confirmed the algorithm's ability to specifically detect hemoglobin even within visually challenging substances, although internal blood detection within stools remains limited.

3.11. Cardiovascular System

Perkov et al. [99] used HSI for the rapid quantitative assessment of infantile hemangiomas (IHs), common benign tumors in infancy. Their system captured images in just 5 s at a high lateral resolution (10 μm), enabling the accurate measurement of hemoglobin oxygenation and vascular dynamics. The authors developed a quantitative biomarker, termed the s-coefficient, based on total hemoglobin distribution to objectively assess the progression of IHs. In clinical testing involving six infants evaluated over multiple visits, the s-coefficient matched clinical assessments in 90% of cases. Sensitivity to motion artifacts need to be addressed in future studies.

3.12. Endocrine Glands

Waterhouse et al. [100] described the first-in-human pilot study investigating the use of snapshot HSI endoscopy for enhancing visualization during the transsphenoidal surgery of pituitary adenomas. The authors developed an HSI endoscope using a compact spectrally resolved detector array that could be integrated easily into existing surgical workflows. In a clinical study involving 12 patients, HSI successfully differentiated adenoma tissue from healthy pituitary tissue despite technical challenges including motion blur and image resolution.

4. Discussion

HSI has emerged as a promising modality for the intraoperative assessment of tissue perfusion in oncological surgeries, offering the non-invasive, contrast-free visualization of physiological parameters. Recent advancements have demonstrated the utility of HSI in enhancing surgical decision making by providing real-time, objective perfusion data, which are crucial for procedures including anastomotic site selection and tumor margin delineation.

The recent studies included in this review further demonstrate the potential clinical value of HSI across various oncological procedures. For brain tumor surgery, innovative approaches integrating HSI with augmented reality and machine learning improved tumor delineation accuracy and intraoperative decision making. In head and neck oncology, endoscopic and machine-learning-enhanced HSI demonstrated improved precision in tumor margin identification, potentially reducing incomplete resections. In gastrointestinal, lung, and liver surgeries, HSI correlated well with postoperative outcomes and serum biomarkers, showing promise for real-time perfusion assessments to predict complications. Similarly, studies in breast reconstruction and radiation dermatitis monitoring indicate the role of HSI in objectively assessing tissue perfusion and injury.

In recent years, HSI has undergone substantial technological advances, particularly in data processing, which has progressed from statistical methods such as principal component analysis (PCA), independent component analysis (ICA), and minimum noise fraction

(MNF) to advanced neural architectures, including CNNs, INNs, and hybrid CNN–GNN models. These developments, combined with improved hardware such as high-speed snapshot HSI cameras, have been crucial for enabling real-time applications in dynamic surgical environments by mitigating motion artifacts caused by organ movement, respiration, and the instability of handheld or laparoscopic systems, although such artifacts remain a significant challenge. For routine clinical adoption, further progress is required in three key areas: (i) the development of faster and more compact hardware sensors, (ii) the design of robust motion-compensation algorithms tailored to surgical dynamics, and (iii) the regulatory-approved integration of neural architectures for real-time spectral interpretation into surgical workflows.

At present, HSI primarily provides information on tissue physiology, such as oxygenation, hemoglobin content, and perfusion, rather than directly assessing tumor aggressiveness or molecular subtype—areas of interest for future research. HSI shows strong potential in multimodal approaches, where its spectral–spatial data on tissue physiology can complement other imaging and molecular methods, as already shown in our review (e.g., [68,72,90]). While current studies on HSI in medicine primarily emphasize technical and procedural advances, evidence on long-term patient outcomes and survival rates remains limited. Nonetheless, by enabling earlier disease detection, more accurate intraoperative guidance, and reduced complication rates, the large-scale clinical implementation of HSI has the potential to improve prognosis and health-related quality of life, a prospect that requires validation in multi-center clinical trials.

Our review has a clear limitation in relying on a purely narrative synthesis. This approach was deliberately chosen due to the substantial heterogeneity of the included studies, which varied in design, patient populations, and outcome measures, rendering structured quantitative or semi-quantitative pooling inappropriate. In addition, imaging parameters such as wavelength ranges and acquisition times were not standardized across studies; where available, these differences were documented but could not be meaningfully compared, further supporting the decision to undertake a narrative rather than pooled analysis. The most significant challenge in the clinical integration of HSI in oncology is the lack of standardized thresholds and imaging protocols. Without universally accepted perfusion thresholds and consistent data interpretation criteria, the clinical utility of HSI remains limited, as variability across institutions and devices undermines comparability and reproducibility. Establishing evidence-based perfusion benchmarks, validated through large-scale, multicenter clinical trials, is crucial to enabling reliable, objective decision-making during oncological procedures, especially in critical applications such as anastomotic site selection or tumor margin delineation.

Although secondary technical challenges, such as motion artifacts, image blur, and spectral resolution trade-offs, also impact the effectiveness of HSI, these issues can be mitigated through ongoing technological advancements and the systematic calibration, characterization, verification, and quality control of devices [42,43,115–120]. Nonetheless, without addressing the primary issue of standardized clinical protocols and perfusion thresholds, these technological improvements will have a limited impact on the clinical utility of HSI. Notably, similar challenges are also encountered when using other biomedical optical imaging techniques within the oncological clinical setting [121,122], as well as with other investigational imaging modalities (e.g., [123–129]).

Beyond technical and clinical performance, the cost-effectiveness of HSI remains a critical factor for its successful clinical translation. Its economic value will ultimately depend on whether HSI demonstrably reduces downstream healthcare expenditures by enabling earlier disease detection, improving surgical precision, and lowering complication or reoperation rates, as suggested by several of the studies included in our review.

Practical barriers include integration into existing surgical workflows, the miniaturization of devices for handheld or laparoscopic use, and the need for real-time data processing without disrupting clinical procedures. Technological innovation, workflow adaptation, and rigorous health–economic evaluations [130] will therefore be essential to establishing HSI as a broadly impactful clinical tool. Another aspect which has until recently been very much overlooked is patient and public involvement in research and health technology assessments [131], particularly in developing novel intraoperative imaging techniques [132]. Effectively integrating patient perspectives at various research stages, from ethics review and participant recruitment strategies to results could strengthen research quality, align studies with patient needs, and broaden overall societal impact.

5. Conclusions

This review offers a comprehensive and up-to-date synthesis of the clinical applications of HSI, emphasizing its potential to provide real-time, contrast-free perfusion monitoring and objective tumor delineation. By systematically addressing both recent technological progress and ongoing limitations, it contributes a critical perspective to the existing body of literature. In conclusion, while HSI is emerging as a valuable modality for real-time, quantitative perfusion assessments in oncologic surgery, its broader clinical implementation hinges on resolving the current limitations, particularly the absence of standardized imaging parameters. Multicenter clinical trials will be essential to validate its utility and ensure integration into surgical decision-making pathways.

Author Contributions: Conceptualization, R.H.; methodology, R.H.; validation, R.H., E.O., T.D. and D.B.; formal analysis, T.D. and E.O.; investigation, R.H.; resources, R.H.; data curation, E.O. and T.D.; writing—original draft preparation, R.H., E.O. and T.D.; writing—review and editing, R.H. and D.B.; visualization, T.D. and E.O.; supervision, R.H.; project administration, R.H.; funding acquisition, R.H. All authors have read and agreed to the published version of the manuscript.

Funding: This research was funded by the Slovenian Research and Innovation Agency, grant number P2-0348.

Data Availability Statement: The data presented in this study are available upon request from the corresponding author.

Conflicts of Interest: The authors declare no conflicts of interest and have no known competing financial interests or personal relationships that could have appeared to influence the work reported in this study. Dušan Babič is an employee of Aresis, d.o.o.

Abbreviations

The following abbreviations are used in this manuscript:

AK	Actinic keratosis
AL	Anastomotic leakage
ALT	Alanine transaminase
AR	Augmented reality
ARD	Acute radiation dermatitis
AUC	Area under the curve
BCC	Basal cell carcinoma
CNN	Convolutional neural network
CTCAE	Common Terminology Criteria for Adverse Events
DIEP	Deep inferior epigastric perforator
HbH	Deoxygenated hemoglobin

GNN	Graph neural network
GPU	Graphics processing unit
HbO_2	Oxygenated hemoglobin
HSI	Hyperspectral imaging
HSI-MIS	Hyperspectral imaging system for minimally invasive surgery
HSI-Open	HyperSpectral imaging system for open surgery
HSI-SCI	Hyperspectral imaging-based skin cancer index
ICA	Independent component analysis
ICG-FA	Indocyanine green fluorescence angiography
IDH	Isocitrate dehydrogenase
IH	Infantile hemangioma
INN	Invertible neural network
IoU	Intersection of union
LiDAR	Light detection and ranging
LSCI	Laser speckle contrast imaging
MF	Mycosis fungoides
MNF	Minimum noise fraction
NCT	National Clinical Trial
NIR	Near infrared
NIR-PI	Near-Infrared Perfusion Index
NSCLC	Non-small cell lung cancer
OHI	Organ Hemoglobin Index
PAI	Photoacoustic imaging
PCA	Principal component analysis
pCLE	Probe-based confocal laser endomicroscopy
PpIX	Protoporphyrin IX
RGB	Red–Green–Blue
ROC	Receiver operating curve
SAVE	Spectrum-Aided Vision Enhancer
SCC	Squamous cell carcinoma
SCLC	Small cell lung cancer
SMF	Submucous fibrosis
StO_2	Tissue oxygen saturation
SVM	Support Vector Machine
THI	Tissue Hemoglobin Index
TI	Thermal imaging
TWI	Tissue Water Index
YOLO	You Only Look Once

Appendix A. Literature Review Methodology

Appendix A.1. Research Question and Objective

The objective of this rapid review was to understand how and to what extent HSI provides quantitative perfusion information that can aid intraoperative or peri-operative decision-making in patients with solid tumors undergoing clinical oncological interventions. The review question was structured according to the PICOS framework (Figure A1). We focused on clinical studies involving human patients with solid tumors (Population) where hyperspectral imaging was applied in vivo during oncological procedures (Intervention), compared against alternative imaging modalities or clinical judgment (Comparator). Outcomes of interest included quantitative perfusion metrics, their predictive value for clinical endpoints, and feasibility or safety of use (Outcomes). Eligible study designs were prospective or retrospective clinical investigations, while reviews, animal studies, ex vivo work, and non-peer-reviewed abstracts were excluded (Study design).

Population	Human patients with a histologically confirmed or clinically presumed solid malignancy undergoing diagnosis, surgery, radiotherapy or reconstructive procedures.
Intervention	HSI (any wavelength range or camera type) applied in vivo for tissue-perfusion assessment during, before or immediately after the oncological procedure.
Comparator	Other perfusion-imaging modalities (e.g., ICG-FA, LSCI, Doppler) or standard clinical judgement when no imaging comparator is used.
Outcomes	Primary outcomes: quantitative perfusion metrics (e.g., StO_2, THI, OHI) and their ability to predict clinical endpoints (e.g., anastomotic leak, flap viability, margin status). Secondary outcomes: diagnostic accuracy, operative decision changes, postoperative complications, feasibility and safety of HIS implementation.
Study design	Prospective or retrospective clinical studies (incl. pilot/feasibility trials); ≥1 human participant. Exclude: reviews, conference abstracts without full peer review, purely ex vivo/animal/methodological papers.

Figure A1. PICOS criteria to define the research questions.

Appendix A.2. Search Strategy

The literature review was conducted and reported in compliance with the PRISMA 2020 Statement [133], a guide for standard reporting of rapid reviews. The date of the search was 9th of June 2025. Search strings in each database with the number of records are summarized in Figures A2 and A3.

	PICOS element	**MEDLINE (PubMed)** **Title, abstract, keywords**	
		Search terms	**Number of hits**
#1	Patients	("Neoplasms"[Mesh] OR cancer*[tiab] OR tumor*[tiab] OR tumour*[tiab] OR carcinoma*[tiab] OR oncology[tiab] OR SCC[tiab] OR BCC[tiab] OR melanoma[tiab])	5,455,248
#2	Intervention	("Hyperspectral Imaging"[Mesh] OR hyperspectral imaging[tiab] OR multispectral imaging[tiab] OR spectral imaging[tiab])	7792
#3	**#1 AND #2**		1301
#4	**#3 + filters**	Filters: Humans; Publication date after 3 October 2022	**186**

Figure A2. Search strategy and number of hits in PubMed.

	PICOS element	**Scopus** **Title, abstract, keywords**	
		Search terms	**Number of hits**
#1	Patients	TITLE-ABS-KEY (cancer* OR tumor* OR tumour* OR carcinoma* OR oncology OR SCC OR BCC OR melanoma)	6,646,777
#2	Intervention	TITLE-ABS-KEY ("hyperspectral imaging" OR "multispectral imaging" OR "spectral imaging")	37,529
#3	**#1 AND #2**		2763
#4	**#3 + filters**	Filters: Publication date 2022 and beyond	**878**

Figure A3. Search strategy and number of hits in Scopus.

Appendix A.3. Screening Methods

Title and abstract screening

Screening was performed by one reviewer, with 20% of titles and abstracts independently checked by a second reviewer to ensure consistency. Discrepancies were resolved by discussion. This streamlined procedure was consistent with recommendations for rapid reviews [134]. Records were excluded if they met any of the following criteria (hierarchical):

1. Non-English or no abstract/title;
2. Non-human study;
3. Not an oncological population;
4. HSI not used as an in vivo perfusion tool;
5. Not an original peer-reviewed article (e.g., conference abstract, review, editorial);
6. Published before 3 October 2022 (outside update window).

Full-text screening

Potentially eligible papers were retrieved in full and assessed by the same primary reviewer, with 20% double-checked. Exclusion reasons were recorded for the PRISMA diagram. Full texts were excluded if they met any of the following criteria, otherwise they were included:

1. Not in English
2. Non-human study
3. Published before 3 October 2022
4. Not an oncological population
5. HSI not used as an in vivo perfusion tool in a clinical setting
6. Not an original article

Additional sources

In addition to the database queries, we manually screened reference lists of key reviews, conference proceedings, and specialist journals. This hand-search yielded a small number of extra records that were not indexed in PubMed or Scopus. These articles were imported into EndNote and processed according to the same de-duplication, screening, and data-extraction workflow described above.

Data extraction

The primary reviewer extracted study characteristics, HSI system details, anatomical site, perfusion metrics, comparators, and key findings into a pre-piloted Excel sheet; in total, 20% of extractions were verified by the second reviewer. Conflicts were resolved by consensus. All steps and exclusions are summarized in a PRISMA-2020 flow diagram (Figure 1).

Screening results

The database search retrieved 1064 records in total (186 from PubMed and 878 from Scopus). After automated and manual de-duplication in EndNote, 872 unique citations remained. Title and abstract screening removed 808 irrelevant or ineligible papers, leaving 64 articles for full-text assessment. Twenty-nine articles satisfied all inclusion criteria at full-text review and were retained for data extraction. A list of exclusion reasons of references at the full-text stage is presented in Figure A4.

Exclusion criteria	Number of records
Not in English	0
Non-human study	6
Published before 3 October 2022	14
Not an oncological population	0
HSI not used as an in vivo perfusion tool in a clinical setting	11
Not an original article	2
Duplicate	2

Figure A4. Exclusion criteria applied at full-text review.

Following the execution of the primary search strategies in PubMed and Scopus, we conducted a brief, targeted supplementary search to minimize the risk of missing recently published or poorly indexed studies. Because this study followed a rapid review approach [134], supplementary searches were conducted in a structured but pragmatic manner. Specifically, Google Scholar and specialist journal searches used the term 'hyperspectral imaging' combined with organ-specific keywords, and the 'related articles' function plus reference lists of included studies were screened. Although such supplementary searches cannot completely exclude the possibility of missed records, this standardized procedure helped ensure that poorly indexed or very recent publications were captured. Through this process, five additional records [68,73,88,95,96] were retrieved and subjected to a simplified screening process. In total, 34 studies (29 from databases and 5 from additional sources) form the evidence base for this rapid review. Figure 1 in the main text presents the PRISMA flow diagram for this rapid review.

Quality Assessment

As rapid review methodology aims to provide a timely overview of emerging applications, we did not use formal quality appraisal tools such as QUADAS-2. This is in line with Cochrane guidance for rapid reviews [134], where critical appraisal may be simplified or omitted depending on resource constraints and objectives. Instead, we transparently reported the study design, sample size, and key methodological features in the Results section, which allows readers to gauge the robustness of the evidence.

References

1. Kamruzzaman, M.; Sun, D.W. Introduction to Hyperspectral Imaging Technology. In *Computer Vision Technology for Food Quality Evaluation*; Elsevier: Amsterdam, The Netherlands, 2016; pp. 111–139. [CrossRef]
2. Li, Q.; He, X.; Wang, Y.; Liu, H.; Xu, D.; Guo, F. Review of spectral imaging technology in biomedical engineering: Achievements and challenges. *J. Biomed. Opt.* **2013**, *18*, 100901. [CrossRef]
3. Bhargava, A.; Sachdeva, A.; Sharma, K.; Alsharif, M.H.; Uthansakul, P.; Uthansakul, M. Hyperspectral imaging and its applications: A review. *Heliyon* **2024**, *10*, e33208. [CrossRef]
4. Cheng, M.-F.; Mukundan, A.; Karmakar, R.; Valappil, M.A.E.; Jouhar, J.; Wang, H.-C. Modern Trends and Recent Applications of Hyperspectral Imaging: A Review. *Technologies* **2025**, *13*, 170. [CrossRef]
5. Chang, C.-I. *Hyperspectral Imaging*; Springer: Boston, MA, USA, 2003. [CrossRef]
6. Richards, J.A.; Jia, X. *Remote Sensing Digital Image Analysis: An Introduction*; Springer: Berlin/Heidelberg, Germany, 2006. [CrossRef]
7. Lu, G.; Fei, B. Medical hyperspectral imaging: A review. *J. Biomed. Opt.* **2014**, *19*, 010901. [CrossRef] [PubMed]
8. Anichini, G.; Leiloglou, M.; Hu, Z.; O'Neill, K.; Elson, D. Hyperspectral and multispectral imaging in neurosurgery: A systematic literature review and meta-analysis. *Eur. J. Surg. Oncol.* **2025**, *51*, 108293. [CrossRef]
9. Zhang, Y.; Wu, X.; He, L.; Meng, C.; Du, S.; Bao, J.; Zheng, Y. Applications of hyperspectral imaging in the detection and diagnosis of solid tumors. *Transl. Cancer Res. TCR* **2020**, *9*, 1265–1277. [CrossRef]
10. Burström, G.; Amini, M.; El-Hajj, V.G.; Arfan, A.; Gharios, M.; Buwaider, A.; Losch, M.S.; Manni, F.; Edström, E.; Elmi-Terander, A. Optical Methods for Brain Tumor Detection: A Systematic Review. *J. Clin. Med.* **2024**, *13*, 2676. [CrossRef]

11. Lai, C.-L.; Karmakar, R.; Mukundan, A.; Natarajan, R.K.; Lu, S.-C.; Wang, C.-Y.; Wang, H.-C. Advancing hyperspectral imaging and machine learning tools toward clinical adoption in tissue diagnostics: A comprehensive review. *APL Bioeng.* **2024**, *8*, 041504. [CrossRef]
12. Kotwal, A.; Saragadam, V.; Bernstock, J.D.; Sandoval, A.; Veeraraghavan, A.; Valdés, P.A. Hyperspectral imaging in neurosurgery: A review of systems, computational methods, and clinical applications. *J. Biomed. Opt.* **2024**, *30*, 023512. [CrossRef]
13. Gioux, S.; Stockdale, A.; Oketokoun, R.; Ashitate, Y.; Durr, N.J.; Moffitt, L.A.; Frangioni, J.V.; Mazhar, A.; Tromberg, B.J.; Durkin, A.J.; et al. First-in-human pilot study of a spatial frequency domain oxygenation imaging system. *J. Biomed. Opt.* **2011**, *16*, 1. [CrossRef]
14. Holzer, M.S.; Best, S.L.; Jackson, N.; Thapa, A.; Raj, G.V.; Cadeddu, J.A.; Zuzak, K.J. Assessment of Renal Oxygenation During Partial Nephrectomy Using Hyperspectral Imaging. *J. Urol.* **2011**, *186*, 400–404. [CrossRef] [PubMed]
15. Sucher, R.; Athanasios, A.; Köhler, H.; Wagner, T.; Brunotte, M.; Lederer, A.; Gockel, I.; Seehofer, D. Hyperspectral Imaging (HSI) in anatomic left liver resection. *Int. J. Surg. Case Rep.* **2019**, *62*, 108–111. [CrossRef] [PubMed]
16. Noordmans, H.J.; Ferrier, C.; De Roode, R.; Leijten, F.; Van Rijen, P.; Gosselaar, P.; Klaessens, J.; Verdaasdonk, R. Imaging the seizure during surgery with a hyperspectral camera. *Epilepsia* **2013**, *54*, e150–e154. [CrossRef] [PubMed]
17. Barberio, M.; Benedicenti, S.; Pizzicannella, M.; Felli, E.; Collins, T.; Jansen-Winkeln, B.; Marescaux, J.; Viola, M.G.; Diana, M. Intraoperative Guidance Using Hyperspectral Imaging: A Review for Surgeons. *Diagnostics* **2021**, *11*, 2066. [CrossRef]
18. Shapey, J.; Xie, Y.; Nabavi, E.; Bradford, R.; Saeed, S.R.; Ourselin, S.; Vercauteren, T. Intraoperative multispectral and hyperspectral label-free imaging: A systematic review of in vivo clinical studies. *J. Biophotonics* **2019**, *12*, e201800455. [CrossRef]
19. Olweny, E.O.; Faddegon, S.; Best, S.L.; Jackson, N.; Wehner, E.F.; Tan, Y.K.; Zuzak, K.J.; Cadeddu, J.A. First Place: Renal Oxygenation During Robot-Assisted Laparoscopic Partial Nephrectomy: Characterization Using Laparoscopic Digital Light Processing Hyperspectral Imaging. *J. Endourol.* **2013**, *27*, 265–269. [CrossRef]
20. Liu, Z.-W.; Faddegon, S.; Olweny, E.O.; Best, S.L.; Jackson, N.; Raj, G.V.; Zuzak, K.J.; Cadeddu, J.A. Renal Oxygenation During Partial Nephrectomy: A Comparison Between Artery-Only Occlusion Versus Artery and Vein Occlusion. *J. Endourol.* **2013**, *27*, 470–474. [CrossRef]
21. Mori, M.; Chiba, T.; Nakamizo, A.; Kumashiro, R.; Murata, M.; Akahoshi, T.; Tomikawa, M.; Kikkawa, Y.; Yoshimoto, K.; Mizoguchi, M.; et al. Intraoperative visualization of cerebral oxygenation using hyperspectral image data: A two-dimensional mapping method. *Int. J. CARS* **2014**, *9*, 1059–1072. [CrossRef]
22. Ravi, D.; Fabelo, H.; Callic, G.M.; Yang, G.-Z. Manifold Embedding and Semantic Segmentation for Intraoperative Guidance With Hyperspectral Brain Imaging. *IEEE Trans. Med. Imaging* **2017**, *36*, 1845–1857. [CrossRef]
23. Mangotra, H.; Srivastava, S.; Jaiswal, G.; Rani, R.; Sharma, A. Hyperspectral imaging for early diagnosis of diseases: A review. *Expert Syst.* **2023**, *40*, e13311. [CrossRef]
24. Klaessens, J.H.G.M.; Nelisse, M.; Verdaasdonk, R.M.; Noordmans, H.J. Non-contact tissue perfusion and oxygenation imaging using a LED based multispectral and a thermal imaging system, first results of clinical intervention studies. In *SPIE Proceedings*; Mahadevan-Jansen, A., Vo-Dinh, T., Grundfest, W.S., Eds.; SPIE: San Francisco, CA, USA, 2013; Volume 8572, p. 857207.
25. Ebner, M.; Nabavi, E.; Shapey, J.; Xie, Y.; Liebmann, F.; Spirig, J.M.; Hoch, A.; Farshad, M.; Saeed, S.R.; Bradford, R.; et al. Intraoperative hyperspectral label-free imaging: From system design to first-in-patient translation. *J. Phys. D Appl. Phys.* **2021**, *54*, 294003. [CrossRef]
26. Regeling, B.; Thies, B.; Gerstner, A.; Westermann, S.; Müller, N.; Bendix, J.; Laffers, W. Hyperspectral Imaging Using Flexible Endoscopy for Laryngeal Cancer Detection. *Sensors* **2016**, *16*, 1288. [CrossRef] [PubMed]
27. Clancy, N.T.; Soares, A.S.; Bano, S.; Lovat, L.B.; Chand, M.; Stoyanov, D. Intraoperative colon perfusion assessment using multispectral imaging. *Biomed. Opt. Express* **2021**, *12*, 7556. [CrossRef] [PubMed]
28. Stergar, J.; Hren, R.; Milanič, M. Design and Validation of a Custom-Made Hyperspectral Microscope Imaging System for Biomedical Applications. *Sensors* **2023**, *23*, 2374. [CrossRef]
29. Ma, L.; Halicek, M.; Zhou, X.; Dormer, J.D.; Fei, B. Hyperspectral microscopic imaging for automatic detection of head and neck squamous cell carcinoma using histologic image and machine learning. In *Medical Imaging 2020: Digital Pathology*; Tomaszewski, J.E., Ward, A.D., Eds.; SPIE: Houston, TX, USA, 2020; p. 31. [CrossRef]
30. Cruz-Guerrero, I.A.; Campos-Delgado, D.U.; Mejía-Rodríguez, A.R.; Leon, R.; Ortega, S.; Fabelo, H.; Camacho, R.; Plaza, M.D.L.L.; Callico, G. Hybrid brain tumor classification of histopathology hyperspectral images by linear unmixing and an ensemble of deep neural networks. *Healthc. Technol. Lett.* **2024**, *11*, 240–251. [CrossRef]
31. Kho, E.; Dashtbozorg, B.; De Boer, L.L.; Van De Vijver, K.K.; Sterenborg, H.J.C.M.; Ruers, T.J.M. Broadband hyperspectral imaging for breast tumor detection using spectral and spatial information. *Biomed. Opt. Express* **2019**, *10*, 4496. [CrossRef]
32. Jong, L.-J.S.; Post, A.L.; Veluponnar, D.; Geldof, F.; Sterenborg, H.J.C.M.; Ruers, T.J.M.; Dashtbozorg, B. Tissue Classification of Breast Cancer by Hyperspectral Unmixing. *Cancers* **2023**, *15*, 2679. [CrossRef]
33. Cinar, U.; Cetin Atalay, R.; Cetin, Y.Y. Human Hepatocellular Carcinoma Classification from H&E Stained Histopathology Images with 3D Convolutional Neural Networks and Focal Loss Function. *J. Imaging* **2023**, *9*, 25. [CrossRef]

34. Giannoni, L.; Marradi, M.; Scibilia, K.; Ezhov, I.; Bonaudo, C.; Artemiou, A.; Toaha, A.; Lange, F.; Caredda, C.; Montcel, B.; et al. Transportable hyperspectral imaging setup based on fast, high-density spectral scanning for in situ quantitative biochemical mapping of fresh tissue biopsies. *J. Biomed. Opt.* **2024**, *29*, 093508. [CrossRef]
35. Trajanovski, S.; Shan, C.; Weijtmans, P.J.C.; De Koning, S.G.B.; Ruers, T.J.M. Tongue Tumor Detection in Hyperspectral Images Using Deep Learning Semantic Segmentation. *IEEE Trans. Biomed. Eng.* **2021**, *68*, 1330–1340. [CrossRef]
36. Halicek, M.; Fabelo, H.; Ortega, S.; Little, J.V.; Wang, X.; Chen, A.Y.; Callico, G.M.; Myers, L.; Sumer, B.D.; Fei, B. Hyperspectral imaging for head and neck cancer detection: Specular glare and variance of the tumor margin in surgical specimens. *J. Med. Imaging* **2019**, *6*, 1. [CrossRef]
37. Halicek, M.; Fabelo, H.; Ortega, S.; Callico, G.M.; Fei, B. In-Vivo and Ex-Vivo Tissue Analysis through Hyperspectral Imaging Techniques: Revealing the Invisible Features of Cancer. *Cancers* **2019**, *11*, 756. [CrossRef] [PubMed]
38. Halicek, M.; Shahedi, M.; Little, J.V.; Chen, A.Y.; Myers, L.L.; Sumer, B.D.; Fei, B. Head and Neck Cancer Detection in Digitized Whole-Slide Histology Using Convolutional Neural Networks. *Sci. Rep.* **2019**, *9*, 14043. [CrossRef]
39. Ortega, S.; Halicek, M.; Fabelo, H.; Callico, G.M.; Fei, B. Hyperspectral and multispectral imaging in digital and computational pathology: A systematic review [Invited]. *Biomed. Opt. Express* **2020**, *11*, 3195. [CrossRef]
40. Tran, M.H.; Ma, L.; Mubarak, H.; Gomez, O.; Yu, J.; Bryarly, M.; Fei, B. Detection and margin assessment of thyroid carcinoma with microscopic hyperspectral imaging using transformer networks. *J. Biomed. Opt.* **2024**, *29*, 093505. [CrossRef] [PubMed]
41. Holmer, A.; Marotz, J.; Wahl, P.; Dau, M.; Kämmerer, P.W. Hyperspectral imaging in perfusion and wound diagnostics—Methods and algorithms for the determination of tissue parameters. *Biomed. Eng./Biomed. Tech.* **2018**, *63*, 547–556. [CrossRef]
42. Stergar, J.; Hren, R.; Milanič, M. Design and Validation of a Custom-Made Laboratory Hyperspectral Imaging System for Biomedical Applications Using a Broadband LED Light Source. *Sensors* **2022**, *22*, 6274. [CrossRef]
43. Gutiérrez-Gutiérrez, J.A.; Pardo, A.; Real, E.; López-Higuera, J.M.; Conde, O.M. Custom Scanning Hyperspectral Imaging System for Biomedical Applications: Modeling, Benchmarking, and Specifications. *Sensors* **2019**, *19*, 1692. [CrossRef]
44. Hren, R.; Sersa, G.; Simoncic, U.; Milanic, M. Imaging perfusion changes in oncological clinical applications by hyperspectral imaging: A literature review. *Radiol. Oncol.* **2022**, *56*, 420–429. [CrossRef]
45. Hren, R.; Stergar, J.; Simončič, U.; Serša, G.; Milanič, M. Assessing Perfusion Changes in Clinical Oncology Applications Using Hyperspectral Imaging. In *9th European Medical and Biological Engineering Conference Proceedings*; Jarm, T., Šmerc, R., Mahnič-Kalamiza, S., Eds.; IFMBE Proceedings; Springer Nature: Cham, Switzerland, 2024; Volume 112, pp. 122–129. [CrossRef]
46. Best, S.L.; Thapa, A.; Jackson, N.; Olweny, E.; Holzer, M.; Park, S.; Wehner, E.; Zuzak, K.; Cadeddu, J.A. Renal Oxygenation Measurement During Partial Nephrectomy Using Hyperspectral Imaging May Predict Acute Postoperative Renal Function. *J. Endourol.* **2013**, *27*, 1037–1040. [CrossRef] [PubMed]
47. Rose, K.; Krema, H.; Durairaj, P.; Dangboon, W.; Chavez, Y.; Kulasekara, S.I.; Hudson, C. Retinal perfusion changes in radiation retinopathy. *Acta Ophthalmol.* **2018**, *96*, e727–e731. [CrossRef]
48. Chin, M.S.; Siegel-Reamer, L.; FitzGerald, G.A.; Wyman, A.; Connor, N.M.; Lo, Y.-C.; Sioshansi, S.; Moni, J.; Giulia Cicchetti, M.; Lalikos, J.F.; et al. Association between cumulative radiation dose, adverse skin reactions, and changes in surface hemoglobin among women undergoing breast conserving therapy. *Clin. Transl. Radiat. Oncol.* **2017**, *4*, 15–23. [CrossRef]
49. Pruimboom, T.; Lindelauf, A.A.M.A.; Felli, E.; Sawor, J.H.; Deliaert, A.E.K.; van der Hulst, R.R.W.J.; Al-Taher, M.; Diana, M.; Schols, R.M. Perioperative Hyperspectral Imaging to Assess Mastectomy Skin Flap and DIEP Flap Perfusion in Immediate Autologous Breast Reconstruction: A Pilot Study. *Diagnostics* **2022**, *12*, 184. [CrossRef] [PubMed]
50. Fabelo, H.; Ortega, S.; Ravi, D.; Kiran, B.R.; Sosa, C.; Bulters, D.; Callicó, G.M.; Bulstrode, H.; Szolna, A.; Piñeiro, J.F.; et al. Spatio-spectral classification of hyperspectral images for brain cancer detection during surgical operations. *PLoS ONE* **2018**, *13*, e0193721. [CrossRef]
51. Fabelo, H.; Halicek, M.; Ortega, S.; Shahedi, M.; Szolna, A.; Piñeiro, J.; Sosa, C.; O'Shanahan, A.; Bisshopp, S.; Espino, C.; et al. Deep Learning-Based Framework for In Vivo Identification of Glioblastoma Tumor using Hyperspectral Images of Human Brain. *Sensors* **2019**, *19*, 920. [CrossRef] [PubMed]
52. Fabelo, H.; Ortega, S.; Szolna, A.; Bulters, D.; Pineiro, J.F.; Kabwama, S.; J-O'Shanahan, A.; Bulstrode, H.; Bisshopp, S.; Kiran, B.R.; et al. In-Vivo Hyperspectral Human Brain Image Database for Brain Cancer Detection. *IEEE Access* **2019**, *7*, 39098–39116. [CrossRef]
53. Fabelo, H.; Ortega, S.; Lazcano, R.; Madroñal, D.; M. Callicó, G.; Juárez, E.; Salvador, R.; Bulters, D.; Bulstrode, H.; Szolna, A.; et al. An Intraoperative Visualization System Using Hyperspectral Imaging to Aid in Brain Tumor Delineation. *Sensors* **2018**, *18*, 430. [CrossRef]
54. Jansen, S.M.; De Bruin, D.M.; Van Berge Henegouwen, M.I.; Bloemen, P.R.; Strackee, S.D.; Veelo, D.P.; Van Leeuwen, T.G.; Gisbertz, S.S. Effect of ephedrine on gastric conduit perfusion measured by laser speckle contrast imaging after esophagectomy: A prospective in vivo cohort study. *Dis. Esophagus* **2018**, *31*, doy031. [CrossRef]
55. Jansen-Winkeln, B.; Maktabi, M.; Takoh, J.P.; Rabe, S.M.; Barberio, M.; Köhler, H.; Neumuth, T.; Melzer, A.; Chalopin, C.; Gockel, I. Hyperspektral-Imaging bei gastrointestinalen Anastomosen. *Chirurg* **2018**, *89*, 717–725. [CrossRef]

56. Jansen-Winkeln, B.; Holfert, N.; Köhler, H.; Moulla, Y.; Takoh, J.P.; Rabe, S.M.; Mehdorn, M.; Barberio, M.; Chalopin, C.; Neumuth, T.; et al. Determination of the transection margin during colorectal resection with hyperspectral imaging (HSI). *Int. J. Color. Dis.* **2019**, *34*, 731–739. [CrossRef]
57. Jansen-Winkeln, B.; Germann, I.; Köhler, H.; Mehdorn, M.; Maktabi, M.; Sucher, R.; Barberio, M.; Chalopin, C.; Diana, M.; Moulla, Y.; et al. Comparison of hyperspectral imaging and fluorescence angiography for the determination of the transection margin in colorectal resections—A comparative study. *Int. J. Color. Dis.* **2021**, *36*, 283–291. [CrossRef]
58. Jansen-Winkeln, B.; Barberio, M.; Chalopin, C.; Schierle, K.; Diana, M.; Köhler, H.; Gockel, I.; Maktabi, M. Feedforward Artificial Neural Network-Based Colorectal Cancer Detection Using Hyperspectral Imaging: A Step towards Automatic Optical Biopsy. *Cancers* **2021**, *13*, 967. [CrossRef]
59. Jansen-Winkeln, B.; Dvorak, M.; Köhler, H.; Maktabi, M.; Mehdorn, M.; Chalopin, C.; Diana, M.; Gockel, I.; Barberio, M. Border Line Definition Using Hyperspectral Imaging in Colorectal Resections. *Cancers* **2022**, *14*, 1188. [CrossRef]
60. Hennig, S.; Jansen-Winkeln, B.; Köhler, H.; Knospe, L.; Chalopin, C.; Maktabi, M.; Pfahl, A.; Hoffmann, J.; Kwast, S.; Gockel, I.; et al. Novel Intraoperative Imaging of Gastric Tube Perfusion during Oncologic Esophagectomy—A Pilot Study Comparing Hyperspectral Imaging (HSI) and Fluorescence Imaging (FI) with Indocyanine Green (ICG). *Cancers* **2021**, *14*, 97. [CrossRef] [PubMed]
61. Köhler, H.; Jansen-Winkeln, B.; Maktabi, M.; Barberio, M.; Takoh, J.; Holfert, N.; Moulla, Y.; Niebisch, S.; Diana, M.; Neumuth, T.; et al. Evaluation of hyperspectral imaging (HSI) for the measurement of ischemic conditioning effects of the gastric conduit during esophagectomy. *Surg. Endosc.* **2019**, *33*, 3775–3782. [CrossRef]
62. Moulla, Y.; Reifenrath, M.; Rehmet, K.; Niebisch, S.; Jansen-Winkeln, B.; Sucher, R.; Hoffmeister, A.; Kreuser, N.; Köhler, H.; Gockel, I. Hybridösophagektomie mit intraoperativem Hyperspektral-Imaging: Videobeitrag. *Chirurg* **2020**, *91*, 1–12. [CrossRef]
63. Pfahl, A.; Radmacher, G.K.; Köhler, H.; Maktabi, M.; Neumuth, T.; Melzer, A.; Gockel, I.; Chalopin, C.; Jansen-Winkeln, B. Combined indocyanine green and quantitative perfusion assessment with hyperspectral imaging during colorectal resections. *Biomed. Opt. Express* **2022**, *13*, 3145. [CrossRef] [PubMed]
64. Schwandner, F.; Hinz, S.; Witte, M.; Philipp, M.; Schafmayer, C.; Grambow, E. Intraoperative Assessment of Gastric Sleeve Oxygenation Using Hyperspectral Imaging in Esophageal Resection: A Feasibility Study. *Visc. Med.* **2021**, *37*, 165–170. [CrossRef]
65. Wagner, T.; Radunz, S.; Becker, F.; Chalopin, C.; Kohler, H.; Gockel, I.; Jansen-Winkeln, B. Hyperspectral imaging detects perfusion and oxygenation differences between stapled and hand-sewn intestinal anastomoses. *Innov. Surg. Sci.* **2022**, *7*, 59–63. [CrossRef] [PubMed]
66. Moulla, Y.; Buchloh, D.C.; Köhler, H.; Rademacher, S.; Denecke, T.; Meyer, H.-J.; Mehdorn, M.; Lange, U.G.; Sucher, R.; Seehofer, D.; et al. Hyperspectral Imaging (HSI)—A New Tool to Estimate the Perfusion of Upper Abdominal Organs during Pancreatoduodenectomy. *Cancers* **2021**, *13*, 2846. [CrossRef]
67. Ayala, L.; Adler, T.J.; Seidlitz, S.; Wirkert, S.; Engels, C.; Seitel, A.; Sellner, J.; Aksenov, A.; Bodenbach, M.; Bader, P.; et al. Spectral imaging enables contrast agent–free real-time ischemia monitoring in laparoscopic surgery. *Sci. Adv.* **2023**, *9*, eadd6778. [CrossRef]
68. Kleiss, S.F.; Michi, M.; Schuurman, S.N.; De Vries, J.-P.P.M.; Werker, P.M.N.; De Jongh, S.J. Tissue perfusion in DIEP flaps using Indocyanine Green Fluorescence Angiography, Hyperspectral imaging, and Thermal imaging. *JPRAS Open* **2024**, *41*, 61–74. [CrossRef]
69. Kondziołka, J.; Michalecki, Ł.; Hajek, J.; Lebiedowska, A.; Hartman-Petrycka, M.; Koprowski, R.; Wilczyński, S. Hemoglobin Concentration as an Indicator of Skin Radiation Damage During Radiation Therapy Treatments. *Int. J. Radiat. Oncol. Biol. Phys.* **2024**, *120*, 1076–1083. [CrossRef]
70. Schimunek, L.; Schöpp, K.; Wagner, M.; Brucker, S.Y.; Andress, J.; Weiss, M. Hyperspectral imaging as a new diagnostic tool for cervical intraepithelial neoplasia. *Arch. Gynecol. Obstet.* **2023**, *308*, 1525–1530. [CrossRef]
71. Vega, C.; Medina, N.; Quintana-Quintana, L.; Leon, R.; Fabelo, H.; Rial, J.; Martín, A.; Callico, G.M. Feasibility study of hyperspectral colposcopy as a novel tool for detecting precancerous cervical lesions. *Sci. Rep.* **2025**, *15*, 820. [CrossRef]
72. Marois, M.; Olson, J.D.; Wirth, D.J.; Elliott, J.T.; Fan, X.; Davis, S.C.; Paulsen, K.D.; Roberts, D.W. A birefringent spectral demultiplexer enables fast hyper-spectral imaging of protoporphyrin IX during neurosurgery. *Commun. Biol.* **2023**, *6*, 341. [CrossRef]
73. Sancho, J.; Villa, M.; Chavarrías, M.; Juarez, E.; Lagares, A.; Sanz, C. SLIMBRAIN: Augmented reality real-time acquisition and processing system for hyperspectral classification mapping with depth information for in-vivo surgical procedures. *J. Syst. Archit.* **2023**, *140*, 102893. [CrossRef]
74. Leon, R.; Fabelo, H.; Ortega, S.; Cruz-Guerrero, I.A.; Campos-Delgado, D.U.; Szolna, A.; Piñeiro, J.F.; Espino, C.; O'Shanahan, A.J.; Hernandez, M.; et al. Hyperspectral imaging benchmark based on machine learning for intraoperative brain tumour detection. *npj Precis. Onc.* **2023**, *7*, 119. [CrossRef]

75. Giannantonio, T.; Alperovich, A.; Semeraro, P.; Atzori, M.; Zhang, X.; Hauger, C.; Freytag, A.; Luthman, S.; Vandebriel, R.; Jayapala, M.; et al. Intra-operative brain tumor detection with deep learning-optimized hyperspectral imaging. In *Optical Biopsy XXI: Toward Real-Time Spectroscopic Imaging and Diagnosis*; Alfano, R.R., Seddon, A.B., Eds.; SPIE: San Francisco, CA, USA, 2023; p. 5.
76. Puustinen, S.; Vrzáková, H.; Hyttinen, J.; Rauramaa, T.; Fält, P.; Hauta-Kasari, M.; Bednarik, R.; Koivisto, T.; Rantala, S.; Von Und Zu Fraunberg, M.; et al. Hyperspectral Imaging in Brain Tumor Surgery—Evidence of Machine Learning-Based Performance. *World Neurosurg.* **2023**, *175*, e614–e635. [CrossRef] [PubMed]
77. MacCormac, O.; Noonan, P.; Janatka, M.; Horgan, C.C.; Bahl, A.; Qiu, J.; Elliot, M.; Trotouin, T.; Jacobs, J.; Patel, S.; et al. Lightfield hyperspectral imaging in neuro-oncology surgery: An IDEAL 0 and 1 study. *Front. Neurosci.* **2023**, *17*, 1239764. [CrossRef] [PubMed]
78. Kifle, N.; Teti, S.; Ning, B.; Donoho, D.A.; Katz, I.; Keating, R.; Cha, R.J. Pediatric Brain Tissue Segmentation Using a Snapshot Hyperspectral Imaging (sHSI) Camera and Machine Learning Classifier. *Bioengineering* **2023**, *10*, 1190. [CrossRef]
79. Martín-Pérez, A.; Martinez De Ternero, A.; Lagares, A.; Juarez, E.; Sanz, C. Spectral analysis comparison of pushbroom and snapshot hyperspectral cameras for in vivo brain tissues and chromophore identification. *J. Biomed. Opt.* **2024**, *29*, 093510. [CrossRef]
80. Pertzborn, D.; Nguyen, H.-N.; Hüttmann, K.; Prengel, J.; Ernst, G.; Guntinas-Lichius, O.; Von Eggeling, F.; Hoffmann, F. Intraoperative Assessment of Tumor Margins in Tissue Sections with Hyperspectral Imaging and Machine Learning. *Cancers* **2022**, *15*, 213. [CrossRef] [PubMed]
81. Bali, A.; Bitter, T.; Mafra, M.; Ballmaier, J.; Kouka, M.; Schneider, G.; Mühlig, A.; Ziller, N.; Werner, T.; Von Eggeling, F.; et al. Endoscopic In Vivo Hyperspectral Imaging for Head and Neck Tumor Surgeries Using a Medically Approved CE-Certified Camera with Rapid Visualization During Surgery. *Cancers* **2024**, *16*, 3785. [CrossRef] [PubMed]
82. Felicio-Briegel, A.; Linek, M.; Sroka, R.; Rühm, A.; Freymüller, C.; Stocker, M.; Baumeister, P.; Reichel, C.; Volgger, V. Hyperspectral imaging for monitoring of free flaps of the oral cavity: A feasibility study. *Lasers Surg. Med.* **2024**, *56*, 165–174. [CrossRef] [PubMed]
83. Thoenissen, P.; Heselich, A.; Al-Maawi, S.; Sader, R.; Ghanaati, S. Hyperspectral Imaging Allows Evaluation of Free Flaps in Craniomaxillofacial Reconstruction. *J. Craniofacial Surg.* **2023**, *34*, e212–e216. [CrossRef]
84. Chand, S.; Namasivayam, K.; Dave, J.; Preejith, S.P.; Jayachandran, S.; Sivaprakasam, M. In-vivo non-contact multispectral oral disease image dataset with segmentation. *Sci. Data* **2024**, *11*, 1298. [CrossRef]
85. Hoxha, D.; Krt, A.; Stergar, J.; Tomanič, T.; Grošelj, A.; Štajduhar, I.; Serša, G.; Milanič, M. Skin Lesion Classification in Head and Neck Cancers Using Tissue Index Images Derived from Hyperspectral Imaging. *Cancers* **2025**, *17*, 1622. [CrossRef]
86. Ellebrecht, D.B.; Kugler, C. Intraoperative Determination of Bronchus Stump and Anastomosis Perfusion with Hyperspectral Imaging. *Surg. Innov.* **2023**, *30*, 314–323. [CrossRef]
87. Felli, E.; Cinelli, L.; Bannone, E.; Giannone, F.; Muttillo, E.M.; Barberio, M.; Keller, D.S.; Rodríguez-Luna, M.R.; Okamoto, N.; Collins, T.; et al. Hyperspectral Imaging in Major Hepatectomies: Preliminary Results from the Ex-Machyna Trial. *Cancers* **2022**, *14*, 5591. [CrossRef]
88. Bannone, E.; Collins, T.; Esposito, A.; Cinelli, L.; De Pastena, M.; Pessaux, P.; Felli, E.; Andreotti, E.; Okamoto, N.; Barberio, M.; et al. Surgical optomics: Hyperspectral imaging and deep learning towards precision intraoperative automatic tissue recognition—Results from the EX-MACHYNA trial. *Surg. Endosc.* **2024**, *38*, 3758–3772. [CrossRef]
89. Calin, M.A.; Manea, D.; Dumitrescu, A.; Parasca, S.V. A hyperspectral index-based approach for in vivo automatic detection of skin tumors from hyperspectral images. *Balneo PRM Res. J.* **2023**, *14*, 640. [CrossRef]
90. Stridh, M.; Dahlstrand, U.; Naumovska, M.; Engelsberg, K.; Gesslein, B.; Sheikh, R.; Merdasa, A.; Malmsjö, M. Functional and molecular 3D mapping of angiosarcoma tumor using non-invasive laser speckle, hyperspectral, and photoacoustic imaging. *Orbit* **2024**, *43*, 453–463. [CrossRef]
91. Parasca, S.V.; Calin, M.A.; Manea, D.; Radvan, R. Hyperspectral imaging with machine learning for in vivo skin carcinoma margin assessment: A preliminary study. *Phys. Eng. Sci. Med.* **2024**, *47*, 1141–1152. [CrossRef] [PubMed]
92. Huang, H.-Y.; Nguyen, H.-T.; Lin, T.-L.; Saenprasarn, P.; Liu, P.-H.; Wang, H.-C. Identification of Skin Lesions by Snapshot Hyperspectral Imaging. *Cancers* **2024**, *16*, 217. [CrossRef] [PubMed]
93. Courtenay, L.A.; Barbero-García, I.; Martínez-Lastras, S.; Del Pozo, S.; Corral De La Calle, M.; Garrido, A.; Guerrero-Sevilla, D.; Hernandez-Lopez, D.; González-Aguilera, D. Near-infrared hyperspectral imaging and robust statistics for in vivo non-melanoma skin cancer and actinic keratosis characterisation. *PLoS ONE* **2024**, *19*, e0300400. [CrossRef] [PubMed]
94. Courtenay, L.A.; Barbero-García, I.; Martínez-Lastras, S.; Del Pozo, S.; Corral, M.; González-Aguilera, D. Using computational learning for non-melanoma skin cancer and actinic keratosis near-infrared hyperspectral signature classification. *Photodiagnosis Photodyn. Ther.* **2024**, *49*, 104269. [CrossRef]

95. Zimmermann, A.; Köhler, H.; Chalopin, C.; Jansen-Winkeln, B.; Nowotny, R.; Schönherr, T.; Mehdorn, M.; Uttinger, K.L.; Thieme, R.; Gockel, I.; et al. The role of intraoperative hyperspectral imaging (HSI) in colon interposition after esophagectomy. *BMC Surg.* **2023**, *23*, 47. [CrossRef]
96. Thomaßen, M.T.; Köhler, H.; Pfahl, A.; Stelzner, S.; Mehdorn, M.; Thieme, R.; Jansen-Winkeln, B.; Gockel, I.; Chalopin, C.; Moulla, Y. In vivo evaluation of a hyperspectral imaging system for minimally invasive surgery (HSI-MIS). *Surg. Endosc.* **2023**, *37*, 3691–3700. [CrossRef]
97. Ilgen, A.; Köhler, H.; Pfahl, A.; Stelzner, S.; Mehdorn, M.; Jansen-Winkeln, B.; Gockel, I.; Moulla, Y. Intraoperative Laparoscopic Hyperspectral Imaging during Esophagectomy—A Pilot Study Evaluating Esophagogastric Perfusion at the Anastomotic Sites. *Bioengineering* **2024**, *11*, 69. [CrossRef]
98. De Winne, J.; Babin, D.; Luong, H.; Luthman, S.; Van Daele, E.; Vanommeslaeghe, H.; Ceelen, W. Real-time assessment of graft oxygenation and perfusion using spectral imaging for improved outcome in esophageal cancer surgery. In *Optical Biopsy XXIII: Toward Real-Time Spectroscopic Imaging and Diagnosis*; Alfano, R.R., Seddon, A.B., Shi, L., Wu, B., Eds.; SPIE: San Francisco, CA, USA, 2025; p. 12.
99. Perkov, S.; Vorobev, V.; Kurochkin, M.A.; Gorodkov, S.; Gorin, D. Rapid low-cost hyperspectral imaging system for quantitative assessment of infantile hemangioma. *J. Biophotonics* **2024**, *17*, e202300375. [CrossRef]
100. Waterhouse, D.J.; Borsetto, D.; Santarius, T.; Tysome, J.R.; Bohndiek, S.E. First-in-human pilot study of snapshot multispectral endoscopy for delineation of pituitary adenoma. *J. Biomed. Opt.* **2025**, *30*, 056002. [CrossRef]
101. Studier-Fischer, A.; Bressan, M.; bin Qasim, A.; Özdemir, B.; Sellner, J.; Seidlitz, S.; Haney, C.M.; Egen, L.; Michel, M.; Dietrich, M.; et al. Spectral characterization of intraoperative renal perfusion using hyperspectral imaging and artificial intelligence. *Sci. Rep.* **2024**, *14*, 17262. [CrossRef]
102. Merdasa, A.; Berggren, J.; Tenland, K.; Stridh, M.; Hernandez-Palacios, J.; Gustafsson, N.; Sheikh, R.; Malmsjö, M. Oxygen saturation mapping during reconstructive surgery of human forehead flaps with hyperspectral imaging and spectral unmixing. *Microvasc. Res.* **2023**, *150*, 104573. [CrossRef]
103. Vandebriel, R.; Luthman, S.; Vunckx, K.; Jayapala, M.; Charle, W.; Solie, L.; De Vleeschouwer, S.; Giannantonio, T.; Alperovich, A.; Zhang, X. Integrating hyperspectral imaging in an existing intra-operative environment for detection of intrinsic brain tumors. In *Advanced Biomedical and Clinical Diagnostic and Surgical Guidance Systems XXI*; Boudoux, C., Tunnell, J.W., Eds.; SPIE: San Francisco, CA, USA, 2023; p. 33. [CrossRef]
104. Greenspan, H. *Medical Image Computing and Computer Assisted Intervention—MICCAI 2023: 26th International Conference, Vancouver, BC, Canada, October 8–12, 2023, Proceedings, Part IX*, 1st ed.; Lecture Notes in Computer Science Series; Springer: Cham, Switzerland, 2023.
105. Roddan, A.; Czempiel, T.; Xu, C.; Xu, H.; Weld, A.; Chalau, V.; Anichini, G.; Elson, D.S.; Giannarou, S. Multimodal imaging platform for enhanced tumor resection in neurosurgery: Integrating hyperspectral and pCLE technologies. *Int. J. CARS* **2025**, *20*, 1087–1096. [CrossRef]
106. Bali, A.; Wolter, S.; Pelzel, D.; Weyer, U.; Azevedo, T.; Lio, P.; Kouka, M.; Geißler, K.; Bitter, T.; Ernst, G.; et al. Real-Time Intraoperative Decision-Making in Head and Neck Tumor Surgery: A Histopathologically Grounded Hyperspectral Imaging and Deep Learning Approach. *Cancers* **2025**, *17*, 1617. [CrossRef] [PubMed]
107. Mostafa, M.L.; Alperovich, A.; Giannantonio, T.; Barz, B.; Zhang, X.; Holm, F.; Navab, N.; Boehm, F.; Schwamborn, C.; Hoffmann, T.K.; et al. Robust Tumor Segmentation with Hyperspectral Imaging and Graph Neural Networks. In *Lecture Notes in Computer Science*; Springer Nature: Cham, Switzerland, 2025; pp. 258–274. [CrossRef]
108. Ellebrecht, D.B. Hyperspectral imaging enables the differentiation of differentially inflated and perfused pulmonary tissue: A proof-of-concept study in pulmonary lobectomies for intersegmental plane mapping. *Biomed. Eng./Biomed. Tech.* **2023**, *68*, 421–426. [CrossRef]
109. Gockel, I.; Jansen-Winkeln, B.; Holfert, N.; Rayes, N.; Thieme, R.; Maktabi, M.; Sucher, R.; Seehofer, D.; Barberio, M.; Diana, M.; et al. Möglichkeiten und Perspektiven der Hyperspektralbildgebung in der Viszeralchirurgie. *Chirurg* **2020**, *91*, 150–159. [CrossRef]
110. Lin, T.-L.; Lu, C.-T.; Karmakar, R.; Nampalley, K.; Mukundan, A.; Hsiao, Y.-P.; Hsieh, S.-C.; Wang, H.-C. Assessing the Efficacy of the Spectrum-Aided Vision Enhancer (SAVE) to Detect Acral Lentiginous Melanoma, Melanoma In Situ, Nodular Melanoma, and Superficial Spreading Melanoma. *Diagnostics* **2024**, *14*, 1672. [CrossRef] [PubMed]
111. Lin, T.-L.; Karmakar, R.; Mukundan, A.; Chaudhari, S.; Hsiao, Y.-P.; Hsieh, S.-C.; Wang, H.-C. Assessing the Efficacy of the Spectrum-Aided Vision Enhancer (SAVE) to Detect Acral Lentiginous Melanoma, Melanoma In Situ, Nodular Melanoma, and Superficial Spreading Melanoma: Part II. *Diagnostics* **2025**, *15*, 714. [CrossRef]
112. Pfahl, A.; Köhler, H.; Thomaßen, M.T.; Maktabi, M.; Bloße, A.M.; Mehdorn, M.; Lyros, O.; Moulla, Y.; Niebisch, S.; Jansen-Winkeln, B.; et al. Video: Clinical evaluation of a laparoscopic hyperspectral imaging system. *Surg. Endosc.* **2022**, *36*, 7794–7799. [CrossRef] [PubMed]

113. MacCormac, O.; Horgan, C.C.; Waterhouse, D.; Noonan, P.; Janatka, M.; Miles, R.; Jacobs, J.; Dockerill, C.; Trotouin, T.; Schizas, A.; et al. Hyperspectral abdominal laparoscopy with real-time quantitative tissue oxygenation imaging: A live porcine study. *Front. Med. Technol.* **2025**, *7*, 1549245. [CrossRef]
114. Ikematsu, H.; Takara, Y.; Nishihara, K.; Kano, Y.; Owaki, Y.; Okamoto, R.; Fujiwara, T.; Takamatsu, T.; Yamada, M.; Tomioka, Y.; et al. Possibility of determining high quantitative fecal occult blood on stool surface using hyperspectral imaging. *J. Gastroenterol.* **2025**, *60*, 77–85. [CrossRef] [PubMed]
115. Stergar, J.; Hren, R.; Milanič, M. Effects of phantom microstructure on their optical properties. *J. Biomed. Opt.* **2024**, *29*, 093502. [CrossRef]
116. Hacker, L.; Wabnitz, H.; Pifferi, A.; Pfefer, T.J.; Pogue, B.W.; Bohndiek, S.E. Criteria for the design of tissue-mimicking phantoms for the standardization of biophotonic instrumentation. *Nat. Biomed. Eng.* **2022**, *6*, 541–558. [CrossRef]
117. Dinh, J.; Yamashita, A.; Kang, H.; Gioux, S.; Choi, H.S. Optical Tissue Phantoms for Quantitative Evaluation of Surgical Imaging Devices. *Adv. Photonics Res.* **2023**, *4*, 2200194. [CrossRef]
118. Naglič, P.; Zelinskyi, Y.; Rogelj, L.; Stergar, J.; Milanič, M.; Novak, J.; Kumperščak, B.; Bürmen, M. Optical properties of PlatSil SiliGlass tissue-mimicking phantoms. *Biomed. Opt. Express* **2020**, *11*, 3753. [CrossRef] [PubMed]
119. Sekar, S.K.V.; Pacheco, A.; Martella, P.; Li, H.; Lanka, P.; Pifferi, A.; Andersson-Engels, S. Solid phantom recipe for diffuse optics in biophotonics applications: A step towards anatomically correct 3D tissue phantoms. *Biomed. Opt. Express* **2019**, *10*, 2090. [CrossRef]
120. Pruitt, K.; Ma, L.; Rathgeb, A.; Gahan, J.C.; Johnson, B.A.; Strand, D.W.; Fei, B. Design and validation of a high-speed hyperspectral laparoscopic imaging system. *J. Biomed. Opt.* **2024**, *29*, 093506. [CrossRef]
121. Hren, R.; Sersa, G.; Simoncic, U.; Milanic, M. Imaging microvascular changes in nonocular oncological clinical applications by optical coherence tomography angiography: A literature review. *Radiol. Oncol.* **2023**, *57*, 411–418. [CrossRef]
122. Hren, R.; Brezar, S.K.; Marhl, U.; Sersa, G. Laser speckle contrast imaging of perfusion in oncological clinical applications: A literature review. *Radiol. Oncol.* **2024**, *58*, 326–334. [CrossRef]
123. Lux, R.L.; Burgess, M.J.; Wyatt, R.F.; Evans, A.K.; Vincent, G.M.; Abildskov, J.A. Clinically practical lead systems for improved electrocardiography: Comparison with precordial grids and conventional lead systems. *Circulation* **1979**, *59*, 356–363. [CrossRef]
124. Hubley-Kozey, C.L.; Mitchell, L.B.; Gardner, M.J.; Warren, J.W.; Penney, C.J.; Smith, E.R.; Horácek, B.M. Spatial Features in Body-Surface Potential Maps Can Identify Patients With a History of Sustained Ventricular Tachycardia. *Circulation* **1995**, *92*, 1825–1838. [CrossRef]
125. SippensGroenewegen, A.; Spekhorst, H.; Van Hemel, N.M.; Kingma, J.H.; Hauer, R.N.; De Bakker, J.M.; Grimbergen, C.A.; Janse, M.J.; Dunning, A.J. Localization of the site of origin of postinfarction ventricular tachycardia by endocardial pace mapping. Body surface mapping compared with the 12-lead electrocardiogram. *Circulation* **1993**, *88*, 2290–2306. [CrossRef]
126. Hren, R.; Horácek, B.M. Value of simulated body surface potential maps as templates in localizing sites of ectopic activation for radiofrequency ablation. *Physiol. Meas.* **1997**, *18*, 373–400. [CrossRef] [PubMed]
127. Hren, R.; Steinhoff, U.; Gessner, C.; Endt, P.; Goedde, P.; Agrawal, R.; Oeff, M.; Lux, R.L.; Trahms, L. Value of Magnetocardiographic QRST Integral Maps in the Identification of Patients at Risk of Ventricular Arrhythmias. *Pacing Clin. Electrophis* **1999**, *22*, 1292–1304. [CrossRef] [PubMed]
128. Bergquist, J.; Rupp, L.; Zenger, B.; Brundage, J.; Busatto, A.; MacLeod, R.S. Body Surface Potential Mapping: Contemporary Applications and Future Perspectives. *Hearts* **2021**, *2*, 514–542. [CrossRef]
129. Roth, B.J. The magnetocardiogram. *Biophys. Rev.* **2024**, *5*, 021305. [CrossRef] [PubMed]
130. Imre, A.; Nagy, B.; Hren, R. Early-stage health technology assessment of a curative gene therapy for multiple sclerosis. *Br. J. Clin. Pharmacol.* 2025; *early view*. [CrossRef]
131. Jakab, I.; Dimitrova, M.; Houÿez, F.; Bereczky, T.; Fövényes, M.; Maravic, Z.; Belina, I.; Andriciuc, C.; Tóth, K.; Piniazhko, O.; et al. Recommendations for patient involvement in health technology assessment in Central and Eastern European countries. *Front. Public Health* **2023**, *11*, 1176200. [CrossRef]
132. MacCormac, O.; Elliot, M.; Whittaker, L.; Bahl, A.; Ségaud, S.; Plowright, A.J.; Winslade, S.; Taylor-Gee, A.; Spencer, B.; Vercauteren, T.; et al. Science for tomorrow's neurosurgery: Insights on establishing a neurosurgery patient group focused on developing novel intra-operative imaging techniques. *Res. Involv. Engagem.* **2024**, *10*, 112. [CrossRef]

133. Page, M.J.; McKenzie, J.E.; Bossuyt, P.M.; Boutron, I.; Hoffmann, T.C.; Mulrow, C.D.; Shamseer, L.; Tetzlaff, J.M.; Akl, E.A.; Brennan, S.E.; et al. The PRISMA 2020 statement: An updated guideline for reporting systematic reviews. *BMJ* **2021**, *372*, n71. [CrossRef] [PubMed]
134. Garritty, C.; Gartlehner, G.; Nussbaumer-Streit, B.; King, V.J.; Hamel, C.; Kamel, C.; Affengruber, L.; Stevens, A. Cochrane Rapid Reviews Methods Group offers evidence-informed guidance to conduct rapid reviews. *J. Clin. Epidemiol.* **2021**, *130*, 13–22. [CrossRef] [PubMed]